

# Effects of scattering and dust grain size on the temperature structure of protoplanetary discs: A three-layer approach

Akio K. Inoue<sup>1\*</sup>, Akinori Oka<sup>2</sup>, and Taishi Nakamoto<sup>2</sup>

<sup>1</sup>College of General Education, Osaka Sangyo University, 3-1-1, Nakagaito, Daito, Osaka 574-8530, Japan

<sup>2</sup>Department of Earth and Planetary Sciences, Tokyo Institute of Technology, Ookayama, Meguro, Tokyo 152-8551, Japan

## ABSTRACT

The temperature in the optically thick interior of protoplanetary discs is essential for the interpretation of millimeter observations of the discs, for the vertical structure of the discs, for models of the disc evolution and the planet formation, and for the chemistry in the discs. Since large icy grains have a large albedo even in the infrared, the effect of scattering of the diffuse radiation in the discs on the interior temperature should be examined. We have performed a series of numerical radiation transfer simulations including isotropic scattering by grains with various typical sizes for the diffuse radiation as well as for the incident stellar radiation. We also have developed an analytic model including isotropic scattering to understand the physics concealed in the numerical results. With the analytic model, we have shown that the standard two-layer approach is valid only for grey opacity (i.e. grain size  $\gtrsim 10 \mu\text{m}$ ) even without scattering. A three-layer interpretation is required for grain size  $\lesssim 10 \mu\text{m}$ . When the grain size is  $0.1\text{--}10 \mu\text{m}$ , the numerical simulations show that isotropic scattering reduces the temperature of the disc interior. This reduction is nicely explained by the analytic three-layer model as a result of the energy loss by scatterings of the incident stellar radiation and of the warm diffuse radiation in the disc atmosphere. For grain size  $\gtrsim 10 \mu\text{m}$  (i.e. grey scattering), the numerical simulations show that isotropic scattering does not affect the interior temperature. This is nicely explained by the analytic two-layer model; the energy loss by scattering in the disc atmosphere is exactly offset by the “green-house effect” due to scattering of the cold diffuse radiation in the interior.

**Key words:** dust, extinction — methods: analytical — methods: numerical — planetary systems: protoplanetary discs — radiative transfer — scattering

## 1 INTRODUCTION

Protoplanetary discs are planet formation sites. We observe the electro-magnetic radiation from the discs to understand their physical conditions, and then, to know the planet formation, especially, its beginning. Property of the radiation from a disc is essentially determined by the structure of the disc. The structure follows the response of the disc to the radiation from the central star. To interpret the radiation from protoplanetary discs, therefore, we should have a robust link between the radiation from the central star and the disc structure, in particular, the temperature structure.

The temperature structure of the discs is also essential for chemical reactions in the discs. The evolution of various molecules in the discs and the exchange of these molecules between the gas phase and the solid phase on grains will be discussed in detail with the ALMA in near

future (e.g., Nomura et al. 2008). The condensation front of icy molecules, so-called ‘snow line’, is also determined by the temperature structure of the discs (e.g., Sasselov & Lecar 2000; Oka et al. 2009). The location of the snow line is very important because it significantly enhances the amount of solid materials to make planetary cores and affects the supply of water to rocky planets. The temperature structure also affects the evolution of the discs themselves. The accretion activity in the discs is supposed to be driven by the magnetorotational instability (e.g., Sano et al. 2000). This requires a certain degree of the ionization of disc materials which depends on the structure of the discs.

A milestone in the research of the vertical temperature structure of protoplanetary discs is the work by Chiang & Goldreich (1997) (hereafter CG97). They proposed a two-layer model consisting of the super-heated layer directly exposed by the stellar radiation and the interior warmed by the super-heated layer. This model explained the shape of the spectral energy distribution of the

\* E-mail: akinoue@las.osaka-sandai.ac.jp

discs very well. The computational cheapness of the analytic approach makes the CG97 model very useful to compare with a large sample of the discs observed. Therefore, some attempts to refine the simple model of CG97 were performed (Chiang et al. 2001; Dullemond, Dominik, & Natta 2001; Dullemond & Natta 2003a; Rafikov & De Colle 2006; Garaud & Lin 2007).

Despite a great success of the CG97 model, numerical simulations of the radiation transfer in the discs showed a significant decrement of the equatorial temperature relative to the prediction by the CG97 model (Dullemond & Natta 2003a). The internal energy loss by the radiation at a long wavelength where the optical depth of the disc is relatively small is suggested as a cause of the decrement (Dullemond et al. 2002; Dullemond & Natta 2003a). In the CG97 model and refined ones, the wavelength dependence of dust opacity was taken into account in terms of mean opacity. Dullemond et al. (2002) argued the importance of using full wavelength dependent opacity. However, we propose an alternative approach in this paper: a three-layer model with mean opacity which reproduces the temperature reduction quite well. In addition, we show that the two-layer approximation in the CG97 model is valid only when the dust opacity is “grey” which is expected if the size of dust grains is larger than about 10  $\mu\text{m}$ .

Effect of scattering on the vertical temperature structure was not considered in the literature very much. Scattering of the stellar radiation was taken into account analytically by Calvet et al. (1991) and numerically by Dullemond & Natta (2003b) who showed that the temperature of the disc interior is slightly reduced by the scattering. How about scattering of the diffuse disc radiation? As the size of grains increases, the scattering albedo increases. In particular, the albedo of large icy grains is close to unity even for the infrared wavelength. This may affect the disc structure significantly. Nevertheless, it has not been examined so far.

This paper discusses the effect of scattering of the diffuse radiation as well as that of the stellar radiation on the vertical temperature structure of protoplanetary discs. Since the albedo depends on the grain size, we examine the scattering effect as a function of the grain size. Although there are 2-D/3-D numerical radiation transfer codes available publicly, most of them have a serious difficulty in solving the radiation equilibrium in very high optical depth ( $\tau \sim 10^6$ ) found in protoplanetary discs (Pascucci et al. 2004; Steinacker, Bacmann, & Henning 2006). The RADICAL developed by Dullemond & Turolla (2000) can solve such a problem without any difficulty thanks to a variable Eddington tensor method. However, it treats scattering of only the stellar radiation. We present a variable Eddington factor code with both scatterings of the stellar radiation and of the diffuse radiation but in a 1-D geometry. We also present an analytic model to interpret the numerical results. This simple model would be very useful to understand the physics determining the temperature structure of protoplanetary discs.

The rest of this paper consists of three sections; in section 2, we develop a numerical radiation transfer code taking into account both of the scatterings but only for isotropic case and show the obtained numerical solutions. In section 3, we construct an analytic model to interpret the numerical

solutions and discuss the physical mechanism determining the temperature structure in protoplanetary discs. In the final section, we summarise our findings.

## 2 NUMERICAL RADIATION TRANSFER WITH SCATTERING

Our method is an extension of the variable Eddington factor method developed by Dullemond et al. (2002); we include isotropic scattering of the diffuse radiation as well as that of the stellar radiation. A disc is divided into many annuli in which the transfer of the diffuse radiation is treated one-dimensionally along the normal axis of each annulus with neglecting the radiation energy transport among annuli. This approximation, so-called 1+1D approximation, would be reasonable in an optically thick disc, but not at the near of the disc inner edge nor in a self-shadowing region (e.g., Dullemond, Dominik, & Natta 2001). The radiation from the central star is separated from the diffuse radiation and is treated with the so-called grazing angle recipe. In this paper, we only consider some single annulus cases in order to feature the effect of the scattering on the temperature structure along the normal axis of the annulus. Therefore, we assume a grazing angle  $\alpha = 0.05$  radian throughout of the paper. The density structure along the normal axis of the annulus is solved to be consistent with the obtained temperature structure assuming the hydrostatic equilibrium. In Appendix A, we describe how to obtain the numerical solution of the diffuse radiation transfer with isotropic scattering in each annulus in detail.

### 2.1 A simple dust model

We adopt a very simple dust model in order to feature the effect of scattering on the temperature structure. The absorption and scattering cross sections per unit gas mass at the wavelength  $\lambda$  are assumed to be

$$\kappa_{\lambda}^{\text{abs}} = \begin{cases} \kappa_0^{\text{abs}} & (\lambda \leq \lambda_c) \\ \kappa_0^{\text{abs}} \left(\frac{\lambda}{\lambda_c}\right)^{-1} & (\lambda > \lambda_c) \end{cases}, \quad (1)$$

and

$$\kappa_{\lambda}^{\text{sca}} = \begin{cases} \kappa_0^{\text{sca}} & (\lambda \leq \lambda_c) \\ \kappa_0^{\text{sca}} \left(\frac{\lambda}{\lambda_c}\right)^{-4} & (\lambda > \lambda_c) \end{cases}, \quad (2)$$

respectively. The single scattering albedo at the wavelength  $\lambda$  is

$$\omega_{\lambda} = \frac{\kappa_{\lambda}^{\text{sca}}}{\kappa_{\lambda}^{\text{abs}} + \kappa_{\lambda}^{\text{sca}}}. \quad (3)$$

The critical wavelength  $\lambda_c$  may be related to a typical grain radius  $a$  as  $\lambda_c = 2\pi a$ . If we consider a spherical grain composed of uniform material, the absorption cross section is expressed as  $\kappa_{\lambda}^{\text{abs}} = (3\mathcal{D}Q_{\lambda}^{\text{abs}})/(4\rho_d a)$ , where  $Q_{\lambda}^{\text{abs}}$  is the absorption cross section normalised by the geometrical cross section  $\pi a^2$ ,  $\rho_d$  is the grain material density, and  $\mathcal{D}$  is the dust-to-gas mass ratio. With the values of  $\mathcal{D} = 10^{-2}$  (Solar system nebula),  $\rho_d = 3 \text{ g cm}^{-3}$  (silicate), and  $Q_{\lambda}^{\text{abs}} \rightarrow 1$  ( $\lambda \rightarrow 0$ ), we obtain the absorption cross section for small wavelengths as

$$\kappa_0^{\text{abs}} = 250 \text{ cm}^2 \text{ g}^{-1} \left(\frac{0.1 \mu\text{m}}{a}\right). \quad (4)$$

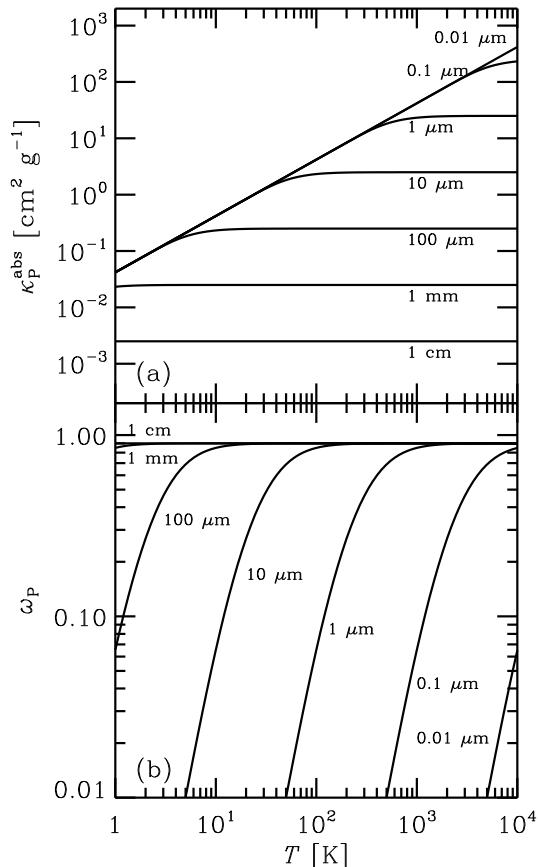


**Figure 1.** Planck mean properties of a simple dust model assumed in this paper: (a) absorption cross section per unit gas mass and (b) single scattering albedo for the case with  $\omega_0 = 0.9$ . We show seven cases of grain size from  $0.01 \mu\text{m}$  to  $1 \text{ cm}$ .

The scattering cross section can be given by the single scattering albedo for small wavelengths:  $\omega_0 = \kappa_0^{\text{sca}} / (\kappa_0^{\text{sca}} + \kappa_0^{\text{abs}})$ . In this paper, we consider three cases of  $\omega_0 = 0$  (no scattering),  $0.9$ , or  $0.99$ . The values of  $\omega_0$  for the last two cases may be extreme but such a large albedo is expected for icy grains in some wavelengths.

Figure 1 shows Planck means of the absorption cross section and the scattering albedo assumed in this paper as a function of the temperature input into the Planck function. In the panels, we show seven cases of grain size from  $0.01 \mu\text{m}$  to  $1 \text{ cm}$ . We note that the absorption cross section and the scattering albedo become independent of the temperature, i.e. “grey”, when the temperature exceeds a critical one which depends on the grain size, corresponds to the critical wavelength  $\lambda_c$ , and is roughly expressed as  $T_c \sim 10^3(1 \mu\text{m}/a) \text{ K}$ . In this paper, we do not consider the size distribution of the dust grains. Thus, the “grain size” of this paper means a typical grain size averaged over a size distribution function with a weight.

## 2.2 Numerical results: Temperature structure

We here show the results of the annulus with the radius of  $1 \text{ AU}$  obtained from our numerical radiation transfer in Figures 2 and 3. The results with other radii have been con-

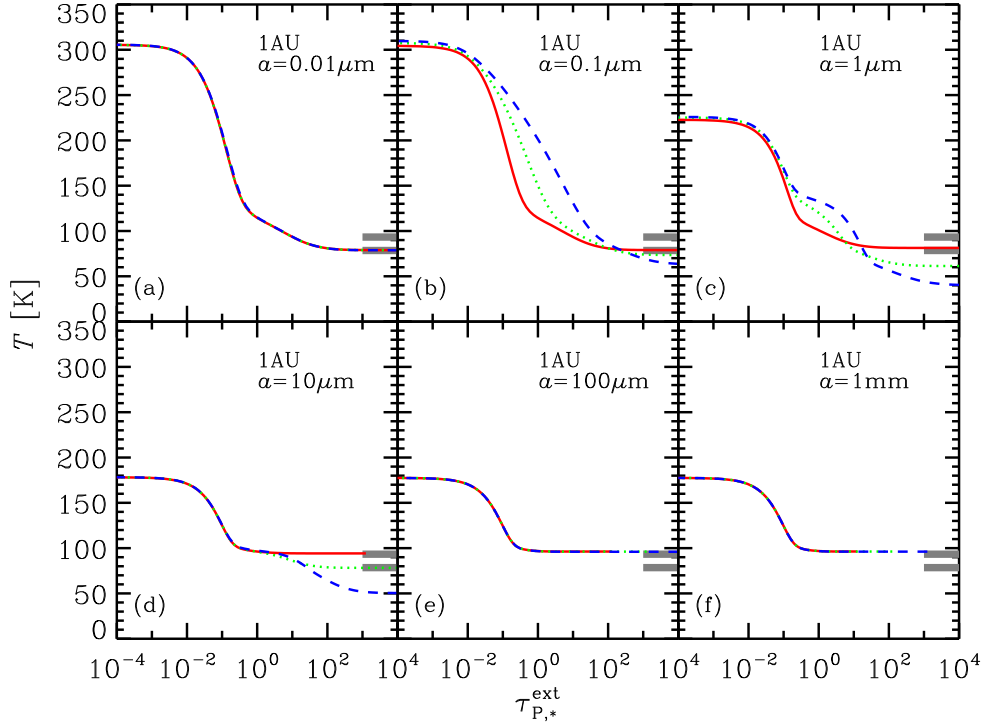
firmed to be the same qualitatively. The gas column density is assumed to be  $10^3(R/\text{AU})^{-1} \text{ g cm}^{-2}$ , where  $R$  is the radial distance from the central star. The properties of the central star assumed are the effective temperature  $T_* = 3,000 \text{ K}$ , the radius  $R_* = 2.0 R_\odot$ , and the mass  $M_* = 0.5 M_\odot$ . Other assumed parameters are as follows: the grazing angle  $\alpha = 0.05$ , the visible fraction of the stellar photosphere at the annuli  $f_{\text{vis}} = 0.5$ , and the mean molecular weight  $\mu_m = 7/3$ .

Figure 2 shows the vertical temperature structures of annuli with  $1 \text{ AU}$  radius with various grain sizes. We take a coordinate of the Planck mean extinction optical depth with the stellar effective temperature as the horizontal axis. Note that the maximum optical depth in each curve occurs the equatorial plane. The grain sizes assumed are shown in each panel. The solid, dotted, and dashed curves are the cases of no scattering (i.e.  $\omega_0 = 0$ ),  $\omega_0 = 0.9$ , and  $\omega_0 = 0.99$ , respectively.

For no scattering cases (solid curves), the so-called two-layer structure proposed by CG97 is confirmed. The dust temperature near the surface is enhanced due to the direct stellar radiation: “super-heated layer”. The thickness of the super-heated layer is well expressed by the Planck mean extinction optical depth as  $\tau_{\text{P},*}^{\text{ext}} \simeq \alpha = 0.05$  (grazing angle). The temperature rapidly decreases if  $\tau_{\text{P},*}^{\text{ext}} > \alpha$ . If the interior is optically thick against its own radiation, then, the interior reaches the thermal equilibrium and becomes isothermal. As the grain size becomes larger, the temperature of the super-heated layer becomes lower. In contrast, the temperature of the interior becomes higher. The physical reason of this phenomenon will be discussed in section 3 with two analytic models: the standard two-layer model like CG97 and a newly developed three-layer model. Here, we just mention the fact that the numerical results agree with the prediction by the three-layer model for the grain size of  $0.01\text{--}1 \mu\text{m}$ , whereas the results agree with that by the two-layer model for the size  $\gtrsim 10 \mu\text{m}$ .

When there is scattering, some differences appear. For  $a = 0.01 \mu\text{m}$  (panel [a]), the scattering albedo  $\omega$  is negligible in the wavelength interest (e.g., an effective temperature less than  $T_* = 3,000 \text{ K}$  in Figure 1). Thus, scattering virtually has no effect. For  $a = 0.1 \mu\text{m}$  (panel [b]),  $\omega$  for the stellar radiation is significant, but that for the diffuse radiation in the annulus (its effective temperature is less than about  $300 \text{ K}$ ) is still negligible (see Figure 1). In this case, the temperature at the equatorial plane becomes slightly lower than that in the no scattering case, which is consistent with Dullemond & Natta (2003b). For  $a = 1\text{--}10 \mu\text{m}$  (panels [c,d]),  $\omega$  becomes significant for the radiation of the super-heated layer. In this case, we observe a plateau like structure at around  $\tau_{\text{P},*}^{\text{ext}} \sim 1$  and a significant reduction of the equatorial temperature. For  $a \gtrsim 100 \mu\text{m}\text{--}1 \text{ mm}$  (panels [e,f]), finally,  $\omega$  becomes “grey” for all the radiation considered here. In this case, the temperature structure with scattering becomes indistinguishable from that without scattering; a “grey” scattering has no effect on the temperature structure in the optical depth coordinate. The physical reasons of these features will be discussed in section 3 with an analytic model.

Even when the “grey” scattering, we find a difference of the temperature structures with/without scattering if we take the physical height as the coordinate as shown in Fig-



**Figure 2.** Vertical temperature structure in annuli with the radius of 1 AU but with various grain sizes,  $a$ , shown in each panel. The horizontal axis is the Planck mean extinction optical depth with the stellar effective temperature ( $T_* = 3,000$  K). The solid lines are the no scattering case, the dotted lines are the case with the single scattering albedo for small wavelength  $\omega_0 = 0.9$ , and the dashed lines are the case with  $\omega_0 = 0.99$ . Two grey thick marks at the right-hand edge in each panel indicate the temperatures predicted by the analytic two-layer (upper mark; 93.3 K) or three-layer (lower mark; 78.5 K) models without scattering presented in section 3.

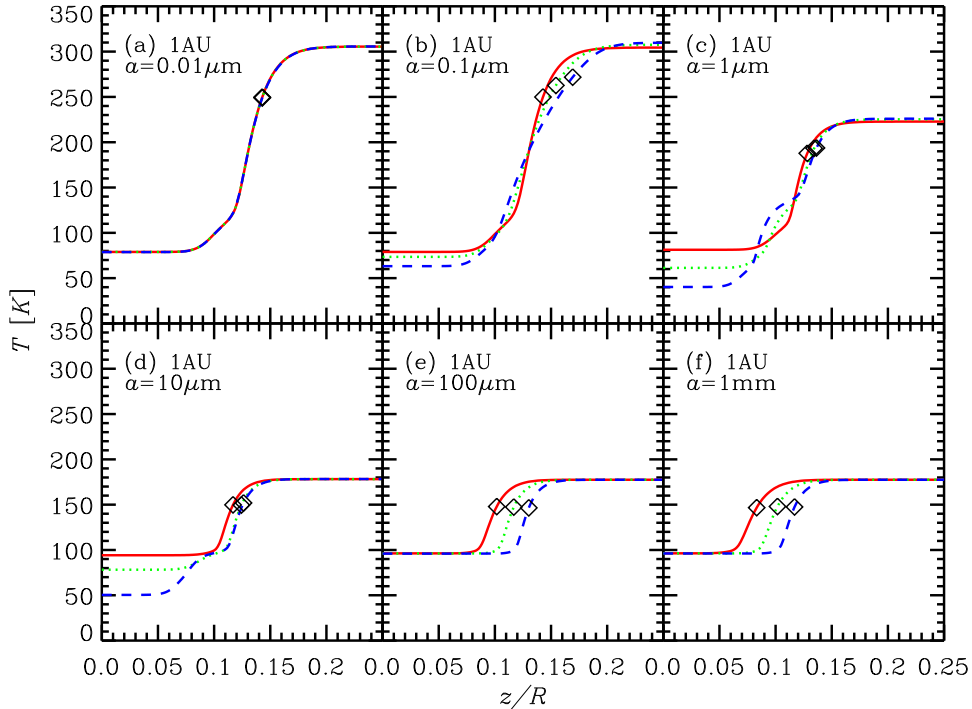


**Figure 3.** Same as Fig. 2, but the horizontal axis is the physical height from the equatorial plane normalised by the radius of the annulus. The diamonds indicate the lower boundary of the super-heated layer, at which the Planck mean extinction optical depth with the stellar effective temperature ( $T_* = 3,000$  K) is equal to the grazing angle ( $\alpha = 0.05$ ).

ure 3. The diamonds in Figure 3 indicate the lower boundary of the super-heated layer, at which the Planck mean extinction optical depth with the stellar effective temperature ( $T_* = 3,000$  K) is equal to the grazing angle. We find that with scattering, the height of the super-heated layer is always enhanced; scattering causes more flaring disc (see also Dullemond & Natta 2003b). This suggests that the scattering may affect the global structure of the disc, which will be discussed in a future work.

### 3 THREE-LAYER ANALYTIC MODEL WITH SCATTERING

In order to understand the numerical results presented in the previous section, we here develop an analytic model as an extension of the seminal two-layer model by CG97: three-layer model with scattering. To describe fluxes across the boundaries of the layers, we adopt a two-stream Eddington approximation with isotropic scattering. The notations in this section are summarised in Table 1.

#### 3.1 Model description

Suppose two or three layers in an annulus as shown in Figure 4. We assume that each layer is isothermal with the temperature determined by the radiation equilibrium in the layer. Then, we consider that each layer emits the radiation characterised by its temperature and other layers just work as absorption and scattering media for the radiation. The radiation from the central star is characterised by the stellar effective temperature. The characterisation of the radiation is done by the Planck mean and the characteristic frequencies are denoted by each subscript such as “\*” for the stellar radiation (see the caption of Figure 4 and Table 1). We denote, for example, the extinction cross section characterised by the stellar effective temperature as  $\kappa_*^{\text{ext}}$ . Note that all the quantities depending on the frequency are Planck averaged in this section.

We call the two or three layers super-heated layer, middle layer, and interior as shown in Figure 4. The super-heated layer is defined as only the layer exposed by the direct stellar radiation entering into the annulus with a small grazing angle  $\alpha$ . The optical thickness of the layer is  $\approx \alpha$  as shown by the numerical solutions in §2.2. Thus, we define the thickness of the super-heated layer as  $\tau_{s,*}^{\text{ext}} \equiv \kappa_*^{\text{ext}} \Sigma_s = \alpha$ , where  $\Sigma_s$  is the gas column density of the layer. The interior represents the isothermal part found in the numerical solutions. Thus, the boundary can be defined by the photosphere of its own radiation. However, we here simply define the interior as the part other than the super-heated and the middle layers.

The middle layer is introduced by the following consideration. When the opacity coefficient decreases as the wavelength increases, the absorption of the radiation from the warm super-heated layer occurs well above the photosphere of the cold interior radiation. In this case, the interior is not warmed directly by the super-heated layer but by the “middle” layer where the radiation of the super-heated layer is effectively absorbed. We here define the thickness of the middle layer as  $\tau_{m,s}^{\text{ext}} \equiv \kappa_s^{\text{ext}} \Sigma_m = 1$  with the gas column density of the middle layer  $\Sigma_m$  although this definition is rather

**Table 2.** Thickness of the upper two layers.

Super-heated layer	$\tau_{s,*}^{\text{ext}} = \alpha$ , i.e. $\Sigma_s = \alpha / \kappa_*^{\text{ext}}$
Middle layer	$\tau_{m,s}^{\text{ext}} = 1$ , i.e. $\Sigma_m = 1 / \kappa_s^{\text{ext}}$

**Table 3.** Condition of the two or three-layer models.

Three-layer model	$\kappa_m^{\text{ext}} / \kappa_s^{\text{ext}} < 1$
Two-layer model	$\kappa_i^{\text{ext}} / \kappa_s^{\text{ext}} \simeq 1$

arbitrary. On the other hand, when the opacity coefficient is grey, the middle layer with the above thickness is optically thick for its own radiation. Thus, the middle layer reaches the thermal equilibrium and is merged into the isothermal interior. In this case, we do not need to consider the middle layer. Therefore, we have two cases: the three-layer model when  $\tau_{m,m}^{\text{ext}} \equiv \kappa_m^{\text{ext}} \Sigma_m < 1$  and the two-layer model when  $\tau_{m,m}^{\text{ext}} \simeq 1$  (or  $\tau_{m,i}^{\text{ext}} \equiv \kappa_i^{\text{ext}} \Sigma_m \simeq 1$  because the middle layer is merged into the interior). In other words, three layers are needed when  $\kappa_m^{\text{ext}} / \kappa_s^{\text{ext}} < 1$  and two layers are sufficient when  $\kappa_i^{\text{ext}} / \kappa_s^{\text{ext}} \simeq 1$ . Tables 2 and 3 are summaries of the thickness of the upper two layers and the condition of the two or three-layer models. Importantly, the seminal two-layer model is valid only when the opacity coefficient is grey in the frequencies interest. This fact has not seemed to be known well so far.

#### 3.1.1 Stellar fluxes

When the grazing angle  $\alpha$  is small, the stellar flux at the top of the annulus is

$$H_*^{\text{in}} = \alpha W_* B_*, \quad (5)$$

with the integrated Planck function  $B_* = (\sigma_{\text{SB}} / \pi) T_*^4$  and the dilution factor  $W_* = \Omega_* / 4\pi$ , where  $\Omega_*$  is the solid angle of the stellar photosphere from the top of the annulus. If only the fraction  $f_{\text{vis}}$  of the stellar photosphere is visible because of the optically thick disc, the solid angle becomes  $\Omega_* = f_{\text{vis}} \pi (R_* / R)^2$ , where  $R_*$  is the stellar radius and  $R$  is the radius of the annulus.

When there is scattering, a part of the incident stellar flux is reflected upwards and downwards by the super-heated layer. Calvet et al. (1991) presented an analytic expression of the scattered flux for isotropic scattering. From equation (5) in Calvet et al. (1991), the outbound fluxes at the upper and lower boundaries of the super-heated layer (see Figure 4) become

$$H_*^{\text{up}} = \alpha W_* B_* \left[ \frac{\omega_*}{1 + \chi_*} \right], \quad (6)$$

and

$$H_*^{\text{down}} = \alpha W_* B_* \left[ \frac{\omega_* \chi_*}{1 + \chi_*} \right], \quad (7)$$

where  $\omega_*$  is the single scattering albedo at the stellar frequency and  $\chi_* = \sqrt{1 - \omega_*}$ . In the derivation of equations (6) and (7), we have assumed  $\tau_{s,*}^{\text{ext}} \equiv \kappa_*^{\text{ext}} \Sigma_s = \alpha \ll 1$ , adopted a different upper boundary condition from Calvet et al.

**Table 1.** Notations in our analytic model.

Notation	Meaning	Remarks
$\alpha$	Grazing angle of the entering stellar radiation	
$\Omega_*$	Solid angle of the stellar photosphere	
$W_*$	Dilution factor of the stellar radiation	$\Omega_*/4\pi$
$H_*^{\text{in}}$	Stellar input flux	
$H_x^{\text{up}}$	Upwards flux from the $x$ layer	
$H_x^{\text{down}}$	Downwards flux from the $x$ layer	
$H_{\text{input}}$	Total downwards flux from the super-heated layer	
$T_x$	Temperature of the $x$ layer	
$B_x$	Frequency integrated Planck function with $T_x$	$(\sigma_{\text{SB}}/\pi)T_x^4$
$\Sigma_x$	Gas mass column density of the $x$ layer	
$\kappa_x^{\text{abs}}$	Absorption cross section per unit gas mass for the radiation with $T_x$	
$\kappa_x^{\text{ext}}$	Extinction cross section per unit gas mass for the radiation with $T_x$	
$\tau_{x,y}^{\text{ext}}$	Extinction optical depth of the $x$ layer for the radiation with $T_y$	$\kappa_y^{\text{ext}}\Sigma_x$
$\omega_x$	Scattering albedo for the radiation with $T_x$	
$\chi_x$	Square-root of the thermal coefficient $1 - \omega_x$	$\sqrt{1 - \omega_x}$
$I_{x,y}^{\text{up}}$	Upwards intensity of the radiation with $T_y$ from the $x$ layer	
$I_{x,y}^{\text{down}}$	Downwards intensity of the radiation with $T_y$ from the $x$ layer	
$a_{x,y}$	Thermal coefficient in the $x$ layer for the radiation with $T_y$	eq. (B13)
$b_{x,y}$	Reflection coefficient in the $x$ layer for the radiation with $T_y$	eq. (B14)
$c_{x,y}$	Transmission coefficient in the $x$ layer for the radiation with $T_y$	eq. (B15)
$\Phi_{\text{input}}$	Ratio of $H_{\text{input}}$ to $H_*^{\text{in}}$	eq. (20)
$\Phi_{i(2)}$	Reduction factor of $B_i$ by scattering in the two-layer model	eq. (23)
$\Phi_{i(3)}$	Reduction factor of $B_i$ by scattering in the three-layer model	eq. (29)

Subscripts  $x$  and  $y$  are \* for stellar quantities, s for super-heated layer quantities, m for middle layer quantities, or i for interior quantities.

$\sigma_{\text{SB}}$  is the Stefan-Boltzmann constant.

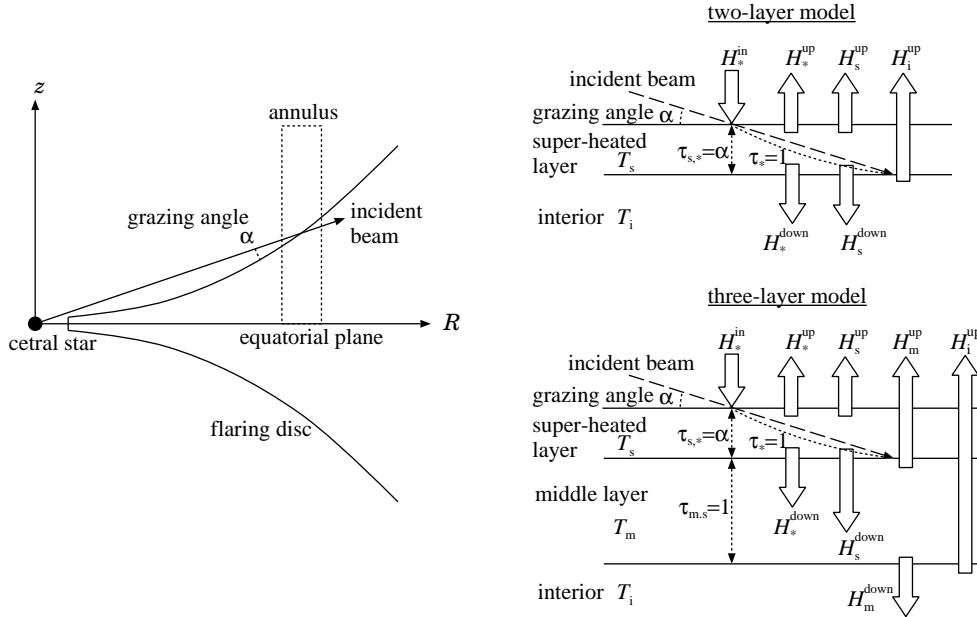


**Figure 4.** Schematic diagram of the two-layer and the three-layer models. We are considering an annulus clipped from a flaring disc surrounding a young star as shown in the left-hand picture. In the annulus, we consider two or three layers as shown in the right-hand pictures. Each layer is assumed to be isothermal with a temperature  $T$ . The fluxes crossing the boundaries of layers are denoted as  $H^{\text{up}}$  or  $H^{\text{down}}$  depending on their direction. We set the direction of arrows in the right-hand pictures as the positive direction for the fluxes. The subscript of each quantity indicates the layer associated with the quantity: “s” for the super-heated layer, “m” for the middle layer, and “i” for the interior. The quantities with the subscript of “\*” are associated with the radiation from the central star and  $H_*^{\text{in}}$  is the stellar flux at the top of the annulus. See also Table 1 for notations.

(1991)<sup>1</sup>, and neglected the term  $e^{-1}$  for the downwards flux. Note that the total scattered flux is  $H_*^{\text{up}} + H_*^{\text{down}} = \omega_* \alpha W_* B_* = \omega_* H_*^{\text{in}}$  and  $H_*^{\text{up}} = H_*^{\text{down}} = 0$  if  $\omega_* = 0$  (no scattering case).

### 3.1.2 Super-heated layer fluxes

The radiation characterised by the temperature of the super-heated layer  $T_s$  is produced only in the super-heated layer. In other layers, this radiation is not produced but is absorbed or scattered. The super-heated layer is vertically optically thin for its own radiation as  $\tau_{s,s}^{\text{ext}} \equiv \kappa_s^{\text{ext}} \Sigma_s = (\kappa_s^{\text{ext}} / \kappa_*^{\text{ext}}) \alpha \ll 1$  because the grazing angle  $\alpha$  is small and we have  $(\kappa_s^{\text{ext}} / \kappa_*^{\text{ext}}) \leq 1$ . On the other hand, the total optical depth of other layers is very large. Thus, we consider a geometry that a thin isothermal layer lies on a semi-infinite absorption and scattering slab.

The above of the super-heated layer is assumed to be vacuum; there is no downwards input radiation with the temperature  $T_s$  at the top of the layer. However, there is upwards input radiation at the bottom of the layer because of the reflection by the semi-infinite interior below the layer. The upwards and downwards radiation intensities from the super-heated layer ( $I_{s,s}^{\text{up}}$  and  $I_{s,s}^{\text{down}}$ , respectively) in the two-stream Eddington approximation (the cosine of the angle between the stream lines and the normal of the layer is set to be  $\pm 1/\sqrt{3}$ ) become from equations (B12) and (B16)

$$I_{s,s}^{\text{up}} = a_{s,s} B_s + c_{s,s} I_{i,s}^{\text{up}}, \quad (8)$$

and

$$I_{s,s}^{\text{down}} = a_{s,s} B_s + b_{s,s} I_{i,s}^{\text{up}}, \quad (9)$$

where  $I_{i,s}^{\text{up}}$  is the upwards input intensity from the interior, and  $a_{s,s}$ ,  $b_{s,s}$ , and  $c_{s,s}$  are the thermal, reflection, and transmission coefficients in the super-heated layer for the radiation characterised by the temperature  $T_s$  (see eqs. [B13–B15]). The reflected intensity from the interior becomes

$$I_{i,s}^{\text{up}} = b_{i,s} I_{s,s}^{\text{down}}, \quad (10)$$

where  $b_{i,s}$  is the reflection coefficient in the interior for the radiation with  $T_s$ . Note that the interior itself does not emit radiation with  $T_s$ .

We can always obtain the unique exact solution of  $I_{s,s}^{\text{up}}$ ,  $I_{s,s}^{\text{down}}$ , and  $I_{i,s}^{\text{up}}$  from equations (8–10), whereas we derive an approximate solution of them in this paper. As found equation (B18), for a semi-infinite slab, we have  $b_{i,s} \approx (1 - \chi_s)/(1 + \chi_s)$ , where  $\chi_s = \sqrt{1 - \omega_s}$  with  $\omega_s$  being the scattering albedo for the radiation with  $T_s$ . Since the super-heated layer is optically thin for its own radiation, we can approximate  $b_{s,s} \ll 1$  and  $c_{s,s} \approx 1$ . We also find  $a_{s,s} \approx \sqrt{3} \chi_s^2 \tau_{s,s}^{\text{ext}} = \sqrt{3} \chi_s^2 (\kappa_s^{\text{ext}} / \kappa_*^{\text{ext}}) \alpha$  from equation (B13) for a small optical depth. Then, we obtain  $I_{s,s}^{\text{up}} \approx (1 + b_{i,s}) a_{s,s} B_s$ ,  $I_{s,s}^{\text{down}} \approx a_{s,s} B_s$ , and  $I_{i,s}^{\text{up}} \approx b_{i,s} a_{s,s} B_s$ . The upwards and downwards fluxes from the super-heated layer are  $H_s^{\text{up}} = I_{s,s}^{\text{up}} / (2\sqrt{3})$  and  $H_s^{\text{down}} = (I_{s,s}^{\text{down}} - I_{i,s}^{\text{up}}) / (2\sqrt{3})$ . Therefore, we obtain

$$H_s^{\text{up}} = \alpha B_s \left( \frac{\kappa_s^{\text{ext}}}{\kappa_*^{\text{ext}}} \right) \left[ \frac{\chi_s^2}{1 + \chi_s} \right], \quad (11)$$

and

$$H_s^{\text{down}} = \alpha B_s \left( \frac{\kappa_s^{\text{ext}}}{\kappa_*^{\text{ext}}} \right) \left[ \frac{\chi_s^3}{1 + \chi_s} \right]. \quad (12)$$

### 3.1.3 Middle layer fluxes

As discussed in the section 3.1, we consider the middle layer only when the layer is optically thin for its own radiation. Although the middle layer is sandwiched between the super-heated layer and the interior, we neglect the effect of the super-heated layer because the optical depth of the layer is very small (see above). The optical depth of the interior is so large that we can regard it as a semi-infinite medium. Thus, we have the same setting as the super-heated layer, other than the optical thickness of the layer,  $\tau_{m,m}^{\text{ext}} = (\kappa_m^{\text{ext}} / \kappa_s^{\text{ext}})$ . Following the section 3.1.2, we have

$$H_m^{\text{up}} = B_m \left( \frac{\kappa_m^{\text{ext}}}{\kappa_s^{\text{ext}}} \right) \left[ \frac{\chi_m^2}{1 + \chi_m} \right], \quad (13)$$

and

$$H_m^{\text{down}} = B_m \left( \frac{\kappa_m^{\text{ext}}}{\kappa_s^{\text{ext}}} \right) \left[ \frac{\chi_m^3}{1 + \chi_m} \right], \quad (14)$$

where  $B_m$  is the integrated Planck function with the temperature of the middle layer  $T_m$ ,  $\omega_m$  is the scattering albedo for the radiation of the middle layer, and  $\chi_m = \sqrt{1 - \omega_m}$ .

### 3.1.4 Interior flux

We always consider the interior to be optically thick for its own radiation. On the other hand, other layers above the interior are considered to be always optically thin. If we neglect the effect of the upper layers, the interior is regarded as a semi-infinite isothermal medium without incident flux of the radiation with the temperature  $T_i$ . In this case, based on equation (B12), the upwards outbound flux becomes  $H_i^{\text{up}} = a_{i,i} B_i / (2\sqrt{3})$  with  $a_{i,i}$  being the thermal coefficient in the interior for the radiation with  $T_i$  and  $B_i$  being the integrated Planck function with  $T_i$ . For a semi-infinite medium,  $a_{i,i} \approx 2\chi_i / (1 + \chi_i)$ , where  $\chi_i = \sqrt{1 - \omega_i}$  with  $\omega_i$  being the single scattering albedo for the interior radiation (eq. [B17]). Therefore, we have

$$H_i^{\text{up}} = \frac{B_i}{\sqrt{3}} \left[ \frac{\chi_i}{1 + \chi_i} \right]. \quad (15)$$

Note that the factor in [ ] is equal or less than 1/2. The equal is true without scattering. Therefore, in general, scattering reduces the radiation energy loss from the interior, i.e. the green-house effect.

## 3.2 Temperature of the super-heated layer

The radiation energy conservation in the super-heated layer is

$$H_*^{\text{in}} - H_*^{\text{up}} - H_*^{\text{down}} = H_s^{\text{up}} + H_s^{\text{down}}. \quad (16)$$

<sup>1</sup> Calvet et al. (1991) adopted  $J(0) = 2H(0)$ , where  $J(0)$  and  $H(0)$  are the mean intensity and the mean flux of the scattered stellar radiation at the top of the medium. On the other hand, we adopted  $J(0) = \sqrt{3}H(0)$ . This difference is due to the choice of the angle of the stream line.

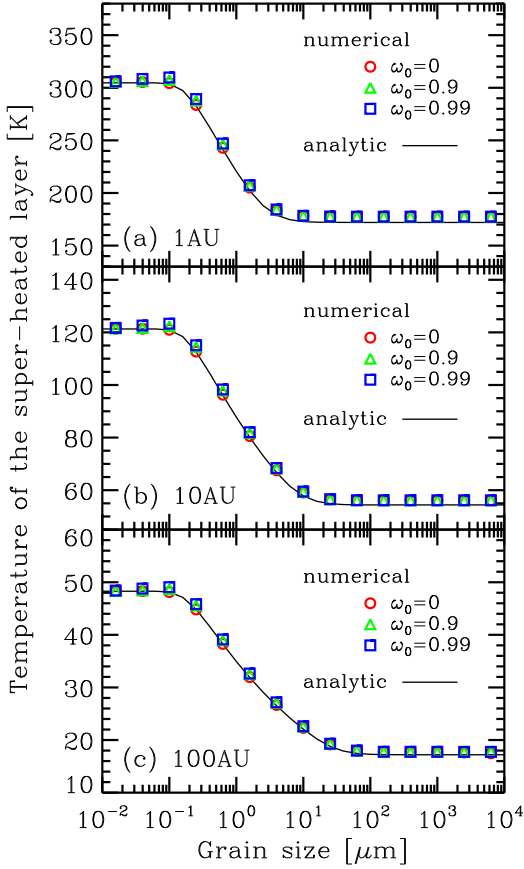


**Figure 5.** Temperature of the super-heated layer as a function of grain size: (a) annulus with the radius of 1 AU, (b) 10 AU, and (c) 100 AU. The numerical solutions are shown by symbols; circles are no scattering case, triangles are the case with the single scattering albedo for small wavelength  $\omega_0 = 0.9$ , and squares are the case with  $\omega_0 = 0.99$ . The solid lines are the analytic model given by equation (18).

The left-hand side is the net input flux of the stellar radiation and becomes  $\alpha W_* B_* (1 - \omega_*)$ . When there is scattering, the input flux is reduced by a factor of  $1 - \omega_*$ . The right-hand side is the net output flux of the super-heated layer and becomes  $\alpha B_s (\kappa_s^{\text{ext}} / \kappa_*^{\text{ext}}) (1 - \omega_s)$ . Thus we obtain

$$B_s = B_* W_* \left( \frac{\kappa_*^{\text{abs}}}{\kappa_s^{\text{abs}}} \right), \quad (17)$$

or

$$T_s = T_* W_*^{1/4} \left( \frac{\kappa_*^{\text{abs}}}{\kappa_s^{\text{abs}}} \right)^{1/4}, \quad (18)$$

where we have applied  $\kappa^{\text{abs}} = (1 - \omega) \kappa^{\text{ext}}$ . Therefore, we expect  $T_s$  to be independent of the existence of scattering. This result can be recovered by a microscopic consideration for each dust grain in the radiation equilibrium with the stellar radiation field in the super-heated layer. We also expect that  $T_s$  shows two asymptotic values since  $(\kappa_*^{\text{abs}} / \kappa_s^{\text{abs}}) = T_* / T_s$  for a small grain size and  $(\kappa_*^{\text{abs}} / \kappa_s^{\text{abs}}) = \text{constant}$  for a large grain size as shown in Figure 1.

Figure 5 shows the temperature of the super-heated layer as a function of grain size. The numerical solutions presented in section 2 are shown by symbols: circles for the no

scattering case, triangles for the  $\omega_0 = 0.9$  case, and squares for the  $\omega_0 = 0.99$  case. The analytic model presented in equation (18) is shown by the solid lines. To obtain the solution  $T_s$  of equation (18), we need an iterative procedure because  $\kappa_s^{\text{abs}}$  depends on  $T_s$ . Figure 5 first shows that the scattering hardly affect  $T_s$  as expected by the analytic model. Indeed, the cases of the three different albedos are superposed for almost all grain sizes, although a temperature enhancement of a few percent is observed in the scattering cases at a grain size of 0.1–1  $\mu\text{m}$ . Figure 5 second shows that the numerical solutions can be divided into two cases: higher temperature for smaller grain size ( $\lesssim 0.1 \mu\text{m}$ ) and lower temperature for larger grain size ( $\gtrsim 10 \mu\text{m}$ ), which is also expected by the analytic model. The agreement between the numerical solutions and the analytic model is excellent although the numerical solutions give about 3% higher temperature than the analytic model. This small difference is probably caused by neglecting the absorption of the interior radiation in the super-heated layer in the analytic model.

### 3.3 Temperature of the interior

We can define the radiation flux input into the interior (including the middle layer) of the annulus as

$$H_{\text{input}} \equiv H_*^{\text{down}} + H_s^{\text{down}} = \alpha W_* B_* \Phi_{\text{input}}, \quad (19)$$

where

$$\Phi_{\text{input}} = \frac{\omega_* \chi_*}{1 + \chi_*} + \frac{\chi_*^2 \chi_s}{1 + \chi_s}, \quad (20)$$

and we have eliminated  $B_s$  by equation (17). If there is no scattering ( $\omega_* = \omega_s = 0$ , i.e.  $\chi_* = \chi_s = 1$ ), we have  $\Phi_{\text{input}} = 1/2$ . That is,  $H_{\text{input}} = \alpha W_* B_* / 2 = H_*^{\text{in}} / 2$ ; a half of the radiation energy received at the top of the annulus is input into the interior (Chiang & Goldreich 1997). For the isotropic scattering case, we always have  $H_{\text{input}} < H_*^{\text{in}} / 2$ ; isotropic scattering always reduces the energy input into the interior relative to the no scattering case (Dullemond & Natta 2003b).

#### 3.3.1 Two-layer model

The energy conservation in the interior under the two-layer model is

$$H_{\text{input}} = H_i^{\text{up}}. \quad (21)$$

From equations (15) and (19), we obtain

$$B_i = \sqrt{3} \alpha W_* B_* \Phi_{i(2)}, \quad (22)$$

where

$$\Phi_{i(2)} = \left( \frac{1 + \chi_i}{\chi_i} \right) \Phi_{\text{input}}. \quad (23)$$

The interior temperature becomes

$$T_i = T_* \left[ \sqrt{3} \alpha W_* \Phi_{i(2)} \right]^{1/4}. \quad (24)$$

Therefore,  $T_i$  is proportional to a factor of  $\Phi_{i(2)}^{1/4}$ . When there is no scattering ( $\Phi_{\text{input}} = 1/2$  and  $\chi_i = 1$ ), we have  $\Phi_{i(2)} = 1$ .

As discussed in section 3.1, the two-layer model is valid if the opacity coefficient is regarded as grey at all the frequencies interest:  $\kappa_i^{\text{ext}} / \kappa_s^{\text{ext}} \simeq 1$ . If this condition is satisfied,



the scattering is also grey;  $\omega_* = \omega_s = \omega_i$  (i.e.  $\chi_* = \chi_s = \chi_i$ ). In this case, we have

$$\Phi_{i(2)} = 1 \quad (\text{no/grey scattering}). \quad (25)$$

Importantly, the factor  $\Phi_{i(2)}$  for grey isotropic scattering is independent of the albedo and equal to the case without scattering. This is caused by the fact that the reduction of the flux input into the interior by scattering ( $\Phi_{\text{input}}$  in eq.[19]) is completely offset by the reduction of the flux out-bound from the interior by scattering ( $(1 + \chi_i)/\chi_i$  in eq.[15]) for grey and isotropic scattering. Therefore, we expect the same interior temperature for grey and isotropic scattering case as that for no scattering case in the two-layer model.

### 3.3.2 Three-layer model

The energy conservations in the middle layer and the interior under the three-layer model are

$$H_{\text{input}} = H_{\text{m}}^{\text{up}} + H_{\text{m}}^{\text{down}}, \quad (26)$$

and

$$H_{\text{m}}^{\text{down}} = H_{\text{i}}^{\text{up}}. \quad (27)$$

Since  $H_{\text{m}}^{\text{down}} = \chi_{\text{m}} H_{\text{m}}^{\text{up}}$  from equations (13) and (14), we obtain  $H_{\text{i}}^{\text{up}} = \chi_{\text{m}}/(1 + \chi_{\text{m}}) H_{\text{input}}$ . Thus,

$$B_{\text{i}} = \sqrt{3}\alpha W_* B_* \Phi_{i(3)}, \quad (28)$$

where

$$\Phi_{i(3)} = \left( \frac{\chi_{\text{m}}}{\chi_{\text{i}}} \right) \left( \frac{1 + \chi_{\text{i}}}{1 + \chi_{\text{m}}} \right) \Phi_{\text{input}}. \quad (29)$$

The interior temperature becomes

$$T_{\text{i}} = T_* [\sqrt{3}\alpha W_* \Phi_{i(3)}]^{1/4}. \quad (30)$$

Therefore,  $T_{\text{i}}$  is proportional to a factor of  $\Phi_{i(3)}^{1/4}$ .

From the discussion in section 3.1, the three layer model is valid when  $\kappa_{\text{m}}^{\text{ext}}/\kappa_{\text{s}}^{\text{ext}} < 1$ . This condition is satisfied when the grain size,  $a$ , is smaller than 10–100  $\mu\text{m}$ . When  $a \lesssim 0.01 \mu\text{m}$ , the scattering albedo is negligible at the all frequencies interest. In this case or the no scattering case ( $\omega_x = 0$ , i.e.  $\chi_x = 1$ ), we have

$$\Phi_{i(3)} = \frac{1}{2} \quad (\text{no scattering}). \quad (31)$$

Comparing this with the two-layer model, we find that  $T_{\text{i}}$  in the three-layer model is reduced by a factor of  $(1/2)^{1/4}$  relative to that in the two-layer model even for no scattering case.

When  $0.01 \lesssim a \lesssim 0.1 \mu\text{m}$ ,  $\omega_i \approx \omega_{\text{m}} \approx \omega_{\text{s}} \approx 0$  ( $\chi_i \approx \chi_{\text{m}} \approx \chi_{\text{s}} \approx 1$ ) but  $\omega_* > 0$  ( $\chi_* < 1$ ). In this case, we have

$$\Phi_{i(3)} = \frac{\chi_*}{2} (2 - \chi_*). \quad (32)$$

Thus, we find  $\Phi_{i(3)} < 1/2$ ; we expect a reduction of  $T_{\text{i}}$  relative to that without scattering. When  $0.1 \lesssim a \lesssim 1-10 \mu\text{m}$ ,  $\omega_i \approx \omega_{\text{m}} \approx 0$  ( $\chi_i \approx \chi_{\text{m}} \approx 1$ ) and  $\omega_{\text{s}} \approx \omega_* > 0$  ( $\chi_{\text{s}} \approx \chi_* < 1$ ). In this case, we have

$$\Phi_{i(3)} = \frac{\chi_*}{1 + \chi_*}. \quad (33)$$

When  $1-10 \lesssim a \lesssim 10-100 \mu\text{m}$ ,  $\omega_i \approx 0$  ( $\chi_i \approx 1$ ) and  $\omega_{\text{m}} \approx \omega_{\text{s}} \approx \omega_* > 0$  ( $\chi_{\text{m}} \approx \chi_{\text{s}} \approx \chi_* < 1$ ). Then, we have

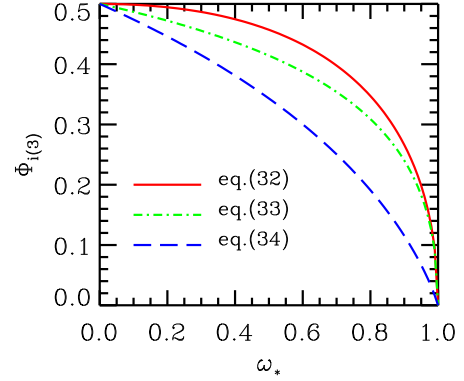


**Figure 6.** Reduction factor of the interior flux by isotropic scattering in the analytic three-layer model,  $\Phi_{i(3)}$ , as a function of the albedo for the stellar radiation,  $\omega_*$ . The solid, dot-dashed, and dashed lines indicate the cases with a typical grain size of  $0.01 \lesssim a \lesssim 0.1 \mu\text{m}$ ,  $0.1 \lesssim a \lesssim 1-10 \mu\text{m}$ , and  $1-10 \lesssim a \lesssim 10-100 \mu\text{m}$ , respectively. The reduction of the interior temperature relative to that in the two-layer model without scattering is given by  $\Phi_{i(3)}^{1/4}$ . Note that the interior temperature in the three-layer model is reduced by a factor of  $(1/2)^{1/4}$  even for  $\omega_* = 0$  (i.e. no scattering).

$$\Phi_{i(3)} = 2 \left( \frac{\chi_*}{1 + \chi_*} \right)^2. \quad (34)$$

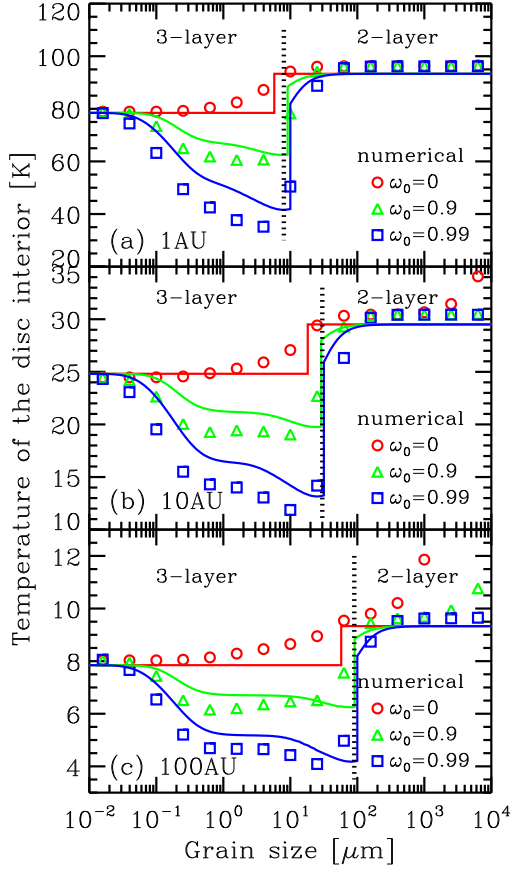
When  $a \gtrsim 10-100 \mu\text{m}$ , the opacity becomes almost grey, thus, the three-layer model is no longer valid. We should choose the two-layer model in this case.

Figure 6 shows the scattering reduction factor  $\Phi_{i(3)}$  given by equations (32–34) as a function of the albedo for the stellar radiation. We find that the factor decreases from equation (32) to (34), in other words, as a function of the grain size. The factor  $\Phi_{i(3)}^{1/4}$  gives the reduction of the interior temperature,  $T_{\text{i}}$ , in the three-layer model by isotropic scattering relative to that in the two-layer model without scattering. For typical grain sizes found in protoplanetary discs of 0.1–10  $\mu\text{m}$ , equation (33) would give a good approximation for the reduction factor. If  $\omega_* \approx 1$ , equations (32) and (33) are reduced to  $\approx \chi_* = \sqrt{1 - \omega_*}$ . In this case, we expect the reduction factor of  $T_{\text{i}}$  to be  $\approx (1 - \omega_*)^{1/8}$  which is found in Figure 7 later.

### 3.3.3 Comparison between numerical and analytic results

Figure 7 shows the temperature of the interior as a function of the grain size. The numerical solutions presented in section 2 are shown by symbols: circles for the no scattering case, triangles for the  $\omega_0 = 0.9$  case, and squares for the  $\omega_0 = 0.99$  case. The analytic models are shown by the solid lines. In analytic models, we always assume the optically thick interior. Most of the numerical solutions shown in Figure 7 are really optically thick. However, when the grain size is larger than about 100  $\mu\text{m}$ , because of the reduction of  $\kappa_0^{\text{abs}}$  given by equation (4), some cases without scattering and with  $\omega_0 = 0.9$  become optically thin. In such cases, we find relatively high temperatures.

The solutions of the analytic models are obtained as



**Figure 7.** Temperature of the disc interior expected in isotropic scattering case as a function of grain size: (a) annulus with the radius of 1 AU, (b) 10 AU, and (c) 100 AU. The numerical solutions are shown by symbols; circles are no scattering case, triangles are the case with the single scattering albedo for small wavelength  $\omega_0 = 0.9$ , and squares are the case with  $\omega_0 = 0.99$ . The solid lines are the analytic model described in sections 3.3.1 (two-layer model; right-hand side) and 3.3.2 (three-layer model; left-hand side). We connect these two models around a grain size indicated by the dotted line, where a jump appears because of this connection (see text in detail). Upwards deviations of numerical solutions from the two-layer model found in panels (b) and (c) are caused by that the interiors of these cases are optically thin for these own radiation.

follows: for the two-layer model, we solved equation (24) to obtain  $T_i$ . We need an iterative procedure because the term  $\Phi_{i(2)}$  depends on  $T_i$ . For the three-layer model, we obtained  $T_i$  from equation (30) after obtaining  $T_m$  from

$$T_m = \left[ \alpha W_* B_* \left( \frac{\kappa_s^{\text{ext}}}{\kappa_m^{\text{abs}}} \right) \Phi_{\text{input}} \right]^{1/4}, \quad (35)$$

which is derived from equations (13), (14), and (26). We again need an iterative procedure to obtain both of  $T_m$  and  $T_i$ .

As discussed in §3.1, the two-layer model is valid only when  $\kappa_i^{\text{ext}}/\kappa_s^{\text{ext}} \approx 1$ . Otherwise, we should adopt the three-layer model. Here, we connect these two models at the grain size where  $\kappa_i^{\text{ext}}/\kappa_s^{\text{ext}} = 0.8$  in the two-layer model, for example; we adopt the two-layer model for a larger grain size than it and adopt the three-layer model for a smaller grain

size than it. This threshold is rather arbitrary, but we find that this choice is good as seen in Figure 7 where the connected analytic models reproduce the numerical solutions reasonably well. Note that a sudden jump on the solid lines in Figure 7 is caused by this connection and numerical solutions also show relatively rapid change of the temperature around there.

When there is no scattering, we find two asymptotic values of  $T_i$ . Interestingly,  $T_i$  for smaller grain size is lower than that for larger grain size, whereas  $T_s$  show the opposite trend in Figure 5. Note that the radiation flux input from the super-heated layer is in fact independent of  $T_s$  as shown in equation (20) in the no scattering case. Nevertheless, the numerical solutions show a factor of  $(1/2)^{1/4}$  reduction of  $T_i$  for small grain cases. This is excellently explained by the three-layer model as found in equation (31). The physical explanation is as follows: when the grain size is small, the radiation flux from the super-heated layer is absorbed by the middle layer once. Then, the middle layer emits a half of the absorbed energy downwards but the rest of the half goes upwards. Therefore, the interior does not receive a half of the stellar radiation energy absorbed by the super-heated layer but receive only a quarter of the energy when the grain size is small.

When there is isotropic scattering, we find further reduction of  $T_i$  in a range of the grain size  $a = 0.1$ –10 or 100  $\mu\text{m}$ . For  $a \sim 0.01$   $\mu\text{m}$ , the scattering effect is not observed because of negligible albedo. For  $a \gtrsim 10$ –100  $\mu\text{m}$ , the scattering effect is not observed, either (but except for the optically thin cases). This is nicely explained by the two-layer model with grey isotropic scattering as found in equation (25). The physical reason is that the grey isotropic scattering equally reduces the downwards flux from the super-heated layer (eq. [19]) and the upwards flux from the interior (eq. [15]). The reduction of  $T_i$  due to scattering for  $a = 0.1$ –10  $\mu\text{m}$  is explained by the three-layer model as summarised in equations (32), (33), and (34). The physical reason of the  $T_i$  reduction is that the scattering reduces only the downwards fluxes from the super-heated layer and from the middle layer because the scattering albedo at the frequency of the interior radiation is still negligible.

## 4 CONCLUSION

We have examined the effect of scattering of the diffuse radiation on the vertical temperature structure of protoplanetary discs. This is motivated by the fact that scattering albedo increases as the size of dust grains grows in the discs. In particular, large icy grains have a significant albedo even in the infrared wavelength. For this aim, we have developed a 1D plane-parallel numerical radiation transfer code including isotropic scattering of the diffuse radiation as well as that of the incident radiation. We have also developed an analytic model with isotropic scattering both of the diffuse and the incident radiations in order to interpret the solutions obtained from the numerical simulation. All results of the numerical simulations has been nicely reproduced by the analytic model.

The analytic model presented in this paper is an extension of the seminal two-layer model by Chiang & Goldreich (1997); we have introduced a new layer between the super-

heated surface layer and the disc interior. This middle layer (or disc atmosphere) is required when the absorption of the radiation from the super-heated layer occurs well above the photosphere of the opaque isothermal interior. This situation is realised if the dust opacity is negatively proportional to the wavelength. Thus, we should consider three layers rather than two layers if the grain size is smaller than about  $10\ \mu\text{m}$ . On the other hand, for grey opacity, which is realised if the grain size is  $\gtrsim 10\ \mu\text{m}$ , the standard treatment with two layers is justified.

We have found from the numerical simulation that the dust temperature of the disc surface is almost not affected by scattering. This is because the temperature is determined by the radiation equilibrium of grains in the incident radiation field locally. The grain size has an effect on the surface temperature via the wavelength dependence of the dust opacity. There are two asymptotic temperatures: the higher temperature is realised by small grains ( $\lesssim 0.1\ \mu\text{m}$ ) and the lower temperature is realised by large grains ( $\gtrsim 1\text{--}10\ \mu\text{m}$ ). This is because the emission efficiency relative to absorption efficiency of the small grains is smaller than that of the large grains which have grey opacity. This trend of the numerical solutions is excellently reproduced by the analytic model of the super-heated layer.

The numerical simulations without scattering show that the dust temperature of the optically thick interior also has two asymptotic values: the lower temperature for small grains ( $\lesssim 0.1\ \mu\text{m}$ ) and the higher temperature for large grains ( $\gtrsim 10\text{--}100\ \mu\text{m}$ ). Thus, the trend is opposite from the surface temperature. The higher asymptotic temperature for large grains is well matched with the prediction of the two-layer model. On the other hand, the lower asymptotic temperature for small grains is a factor of  $(1/2)^{1/4}$  lower than the prediction of the two-layer model. In fact, the flux input from the super-heated layer is always same although the interior temperature is different as a function of the grain size. This phenomenon has been already found by Dullemond & Natta (2003a) who attributed it to the energy loss from the interior by the radiation at a long wavelength (see also Dullemond et al. 2002). We have proposed another interpretation by the middle layer between the super-heated layer and the interior; the super-heated layer gives a half of the absorbed energy of the incident radiation to the middle layer which gives a half of the obtained energy to the interior. This three-layer model exactly predicts a factor of  $(1/2)^{1/4}$  reduction of the interior temperature for the small grain case.

The numerical simulations with isotropic scattering also show two asymptotic temperatures of the interior. Interestingly, these asymptotic temperatures of no scattering and isotropic scattering cases are the same. For small grains ( $\lesssim 0.1\ \mu\text{m}$ ), since the scattering albedo is negligible for all wavelengths interest, the same temperature is trivial. The same temperature for large grains ( $\gtrsim 10\text{--}100\ \mu\text{m}$ ) has been nicely explained by the two-layer model with grey opacity. The physical mechanism is the exact offset between the reduction of the flux input into the interior by scattering in the super-heated layer and the reduction of the flux output from the interior by scattering in itself (i.e. green-house effect).

For grain sizes of  $0.1\text{--}10\ \mu\text{m}$ , which are expected by a moderate growth of the size in the discs, we have found a further reduction of the interior temperature in isotropic scat-

tering cases relative to that without scattering from the numerical simulations. This reduction has been well explained by the three-layer analytic model. The physical mechanism is the wavelength dependence of albedo; the flux input into the interior is reduced by scattering in the super-heated and middle layers, whereas the flux output from the interior is not reduced because of negligible (or weak) scattering. Note that the interior flux has a longer wavelength typically, thus, the albedo for the radiation is smaller.

In conclusion, the scattering of the diffuse radiation can affect the vertical temperature structure of protoplanetary discs significantly when the grain size grows to be about  $1\text{--}10\ \mu\text{m}$ . We need to investigate the effect in a global disc model in future. The analytic model presented in this paper could be useful to understand the physics determining the temperature structure in the discs.

## ACKNOWLEDGMENTS

We would appreciate comments from the anonymous referee which were very useful for us to improve the quality of this paper. AKI is grateful to all members of the Department of Physics, Nagoya University, especially the  $\Omega$  Laboratory led by Tsutomu T. Takeuchi, for their hospitality during this work. AKI is supported by KAKENHI (the Grant-in-Aid for Young Scientists B: 19740108) by The Ministry of Education, Culture, Sports, Science and Technology (MEXT) of Japan.

## REFERENCES

- Calvet, N., Patino, A., Magris, G. C., D'Alessio, P., 1991, *ApJ*, 380, 617
- Chiang, E. I., Goldreich, P., 1997, *ApJ*, 490, 368
- Chiang, E. I., Joungh, M. K., Creech-Eakman, M. J., Qi, C., Kessler, J. E., Blake, G. A., van Dishoeck, E. F., 2001, *ApJ*, 547, 1077
- D'Alessio, P., Calvet, N., Hartmann, L., Franco-Hernández, R., Servín, H., 2006, *ApJ*, 638, 314
- Draine, B. T., 2003, *ARA&A*, 41, 241
- Draine, B. T., Lee, H.-M., 1984, *ApJ*, 285, 89
- Dullemond, C. P., Turolla, R., 2000, *A&A*, 360, 1187
- Dullemond, C. P., Dominik, C., Natta, A., 2001, *ApJ*, 560, 957
- Dullemond, C. P., van Zadelhoff, G. J., Natta, A., 2002, *A&A*, 389, 464
- Dullemond, C. P., Natta, A., 2003a, *A&A*, 405, 597
- Dullemond, C. P., Natta, A., 2003b, *A&A*, 408, 161
- Garaud, P., Lin, D. N. C., 2007, *ApJ*, 654, 606
- Miyake, K., Nakagawa, Y., 1993, *Icarus*, 106, 20
- Ng, K., 1974, *J. Chem. Phys.*, 61, 2680
- Nomura, H., Aikawa, Y., Nakagawa, Y., Millar, T. J., 2008, *A&A*, in press (arXiv:0810.4610)
- Oka, A., Nakamoto, T., et al. 2009, in preparation
- Olson, G. L., Kunasz, P. B., 1987, *JQSRT*, 38, 325
- Pascucci, I., Wolf, S., Steinacker, J., Dullemond, C. P., Henning, Th., Niccolini, G., Woitke, P., Lopez, B., 2004, *A&A*, 417, 793
- Rafikov, R. R., De Colle, F., 2006, *ApJ*, 646, 275

- Rybicki, G. B., Lightman, A. P., 1979, *Radiative Processes in Astrophysics*, Wiley-Interscience, New York
- Sano, T., Miyama, S., Umebayashi, T., Nakano, T., 2000, *ApJ*, 543, 486
- Sasselov, D. D., Lecar, M., 2000, *ApJ*, 528, 995
- Steinacker, J., Bacmann, A., Henning, Th., 2006, *ApJ*, 645, 920
- Strittmatter, P. A., 1974, *A&A*, 32, 7

## APPENDIX A: VARIABLE EDDINGTON FACTOR METHOD WITH ISOTROPIC SCATTERING IN PLANE-PARALLEL SLAB

We here present our numerical radiation transfer method in a plane-parallel medium in detail. The method is based on that developed by Dullemond et al. (2002), but is extended to treat isotropic scatterings of both of the incident radiation (from the central star) and the diffuse radiation (from dust grains in the medium). We find a solution, in which the radiation field, the temperature structure, and the density structure are consistent with each other, iteratively as the following procedure:

- (i) assuming an initial temperature structure
- (ii) solving the density structure consistent with the given temperature structure under the hydrostatic equilibrium
- (iii) solving the transfer of the incident (stellar) radiation with the grazing angle recipe
- (iv) solving the transfer of the diffuse radiation with a variable Eddington factor method and obtaining the temperature structure under the radiation equilibrium
- (v) checking the convergence of the temperature structure and if not going back to the step (ii)

In the following we describe the set of equations and assumptions and the result of a benchmark test.

### A1 Hydrostatic equilibrium

Suppose an annulus clipped from a protoplanetary disk to be a plane-parallel medium. We set the coordinate  $z$  as the vertical height of the medium. The origin  $z = 0$  is the equatorial plane of the annulus and we set a mirror boundary condition there. Assuming the vertical hydrostatic equilibrium, we obtain the density of gas in the medium  $\rho(z)$  consistent with the temperature structure  $T(z)$  which is assumed as an initial guess or is obtained by the previous step of the iteration. We assume that the gas temperature is the same as the dust temperature which is determined by the radiation equilibrium. This assumption is usually well established in the protoplanetary disc because the collision between gas particles and dust grains occurs enough frequently.

The vertical hydrostatic equilibrium is given by

$$\frac{dP}{dz} = -\rho g, \quad (\text{A1})$$

where  $P$  is the gas pressure and  $g$  is the gravitational acceleration. In a protoplanetary disc, the self-gravity of the disc is negligible relative to the gravity of the central star. Thus, we have  $g = GM_*z/R^3$ , where  $G$  is the gravitational constant,  $M_*$  is the mass of the central star, and  $R$  is the distance from the star (or radius of the annulus considered).

We have assumed  $R \gg z$ . The gas pressure is given by the equation of state for the ideal gas as  $P = (\rho k_B T)/(\mu_m m_p)$ , where  $\mu_m$  is the mean molecular weight,  $m_p$  is the proton mass, and  $k_B$  is the Boltzmann constant. Then, equation (A1) is reduced to

$$\frac{d \ln \rho}{dz} = - \left( \frac{\mu m_p}{k_B T} \right) \left( \frac{GM_*}{R^3} \right) z + \frac{d \ln T}{dz}. \quad (\text{A2})$$

If we integrate equation (A2) from  $z = 0$  with a given  $T(z)$ , we obtain the functional shape of  $\rho(z)$ . The absolute value of  $\rho(z)$  is scaled by

$$\Sigma = 2 \int_0^{z_{\max}} \rho(z) dz, \quad (\text{A3})$$

where  $\Sigma$  is the gas column density and  $z_{\max}$  is the maximum height for the numerical calculation. We set  $z_{\max} = R$  in our calculation and we set the minimum value of  $\rho = 10^{-25} \text{ g cm}^{-3}$  just for avoiding a too small value of the density.

We set the optical depth coordinate  $\tau$  for the radiation transfer from the obtained  $\rho(z)$  as

$$\tau_\nu(z) = \int_z^{z_{\max}} \rho(z) \kappa_\nu^{\text{ext}} dz, \quad (\text{A4})$$

where  $\kappa_\nu^{\text{ext}}$  is the extinction cross section by dust grains per unit gas mass at the frequency  $\nu$ .

In fact, we can obtain the temperature structure as a function of the optical depth  $T(\tau)$  by the radiation transfer without the density structure as a function of the vertical height  $\rho(z)$ . The reason why we calculate  $\rho(z)$  and the relation between the optical depth and the vertical height  $\tau(z)$  is to see  $T(z)$  as shown in Figure 3. Another reason, which may be more important, is to determine the grazing angle consistent with the disc global structure for future calculations.

### A2 Transfer of the incident radiation

Let us consider an incident radiation beam entering the plane-parallel medium. The angle between the incident ray and the surface of the medium is called the grazing angle,  $\alpha$ . In a protoplanetary disc, the grazing angle  $\alpha$  is usually as small as  $\sim 0.05$  radian (e.g., D'Alessio et al. 2006). Thus, we use the approximation  $\sin \alpha \approx \alpha$ . The optical depth along the incident ray becomes  $\tau_\nu(z)/\alpha$ . Thus, the mean intensity of the (direct) incident radiation is given by

$$J_\nu^*(z) = J_\nu^{*\max} e^{-\tau_\nu(z)/\alpha}, \quad (\text{A5})$$

where  $J_\nu^{*\max}$  is the mean intensity at the top of the medium (i.e.  $z = z_{\max}$ ). For the incident radiation from the central star,  $J_\nu^{*\max} = B_\nu(T_*)\Omega_*/4\pi$ , where  $B_\nu(T_*)$  is the Planck function with the stellar effective temperature  $T_*$  and  $\Omega_* = \pi(R_*/R)^2 f_{\text{vis}}$  is the solid angle of the stellar photosphere visible from the top of the medium ( $f_{\text{vis}}$  is the visible fraction of the stellar photosphere). Finally, we give the absorbed and extincted energy density of the incident radiation per unit time interval at the height  $z$  as

$$q_{\text{abs}}(z) = \int_0^\infty \rho(z) \kappa_\nu^{\text{abs}} 4\pi J_\nu^* d\nu, \quad (\text{A6})$$

and

$$q_{\text{ext}}(z) = \int_0^\infty \rho(z) \kappa_\nu^{\text{ext}} 4\pi J_\nu^* d\nu, \quad (\text{A7})$$

where  $\kappa_\nu^{\text{abs}}$  and  $\kappa_\nu^{\text{ext}}$  are the absorption and the extinction cross section by dust per unit gas mass at the frequency  $\nu$ .

### A3 Transfer of the diffuse radiation

The transfer equation of the diffuse radiation (or the radiation reprocessed by dust) in a plane-parallel medium is

$$\mu \frac{dI_{\nu\mu}}{dz} = -\rho\kappa_\nu^{\text{ext}} I_{\nu\mu} + \rho\kappa_\nu^{\text{ext}} S_\nu, \quad (\text{A8})$$

where  $\mu$  is the cosine of the angle between the ray and the  $z$  coordinate,  $I_{\nu\mu}$  is the specific intensity at the frequency  $\nu$  towards the direction  $\mu$ , and  $S_\nu$  is the source function which is given by

$$S_\nu = (1 - \omega_\nu) B_\nu(T) + \omega_\nu J_\nu + \omega_\nu J_\nu^*, \quad (\text{A9})$$

where  $\omega_\nu$  is the single scattering albedo at the frequency  $\nu$ ,  $B_\nu(T)$  is the Planck function with the dust temperature  $T$ , and  $J_\nu$  is the mean intensity of  $I_{\nu\mu}$ , that is,  $J_\nu = \frac{1}{2} \int_{-1}^1 I_{\nu\mu} d\mu$ . We have assumed that the scattering is isotropic for the simplicity. Note that we consider the scattering of the diffuse radiation as the second term in equation (A9). The third term accounts for the scattering of the incident radiation. To determine the dust temperature  $T$ , we assume the radiation equilibrium as

$$\int_0^\infty \rho\kappa_\nu^{\text{abs}} B_\nu(T) d\nu = \int_0^\infty \rho\kappa_\nu^{\text{abs}} J_\nu d\nu + \frac{q_{\text{abs}}}{4\pi}. \quad (\text{A10})$$

To obtain the mean intensity  $J_\nu$ , we adopt a variable Eddington factor method. The first and second moments of equation (A8) are

$$\frac{dH_\nu}{dz} = \rho\kappa_\nu^{\text{abs}} (B_\nu - J_\nu) + \rho\kappa_\nu^{\text{sca}} J_\nu^*, \quad (\text{A11})$$

and

$$\frac{dK_\nu}{dz} = -\rho\kappa_\nu^{\text{ext}} H_\nu, \quad (\text{A12})$$

where  $H_\nu = \frac{1}{2} \int_{-1}^1 I_{\nu\mu} \mu d\mu$  and  $K_\nu = \frac{1}{2} \int_{-1}^1 I_{\nu\mu} \mu^2 d\mu$ , and we have used equation (A9) to eliminate  $S_\nu$ . Note that  $\kappa_\nu^{\text{abs}} = (1 - \omega_\nu)\kappa_\nu^{\text{ext}}$  and the scattering cross section per unit gas mass  $\kappa_\nu^{\text{sca}} = \omega_\nu\kappa_\nu^{\text{ext}}$ . If we integrate equations (A11) and (A12) over the frequency, we obtain

$$\frac{dH}{dz} = \frac{q_{\text{ext}}}{4\pi}, \quad (\text{A13})$$

and

$$\frac{dK}{dz} = - \int_0^\infty \rho\kappa_\nu^{\text{ext}} H_\nu d\nu, \quad (\text{A14})$$

where  $H = \int_0^\infty H_\nu d\nu$  and  $K = \int_0^\infty K_\nu d\nu$ , and we have used the radiation equilibrium (eq.[A10]) and equations (A6) and (A7) in equation (A13). Finally, we introduce the Eddington factor as the closure equation:

$$f_E = \frac{K}{J}, \quad (\text{A15})$$

where  $J = \int_0^\infty J_\nu d\nu$ .

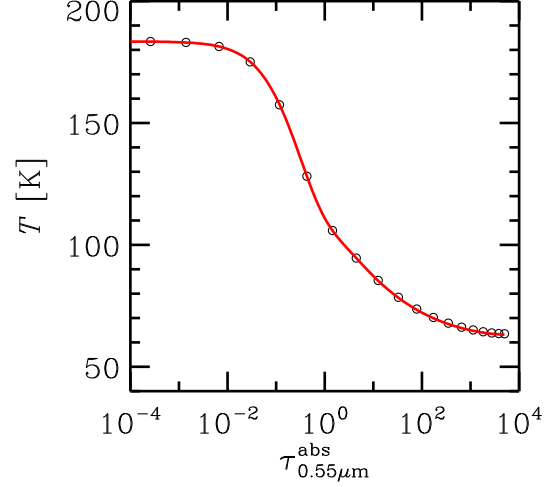


**Figure A1.** Result of a benchmark test without scattering proposed by C. P. Dullemond. The circles are the reference solutions by C. P. Dullemond, whereas the solid line is our solution.

We do not assume  $f_E = 1/3$  (constant) as in the usual Eddington approximation, but obtain  $f_E$  directly from  $I_{\nu\mu}$  which is calculated by the formal solution of equation (A8). The integration of the formal solution is performed with a parabolic interpolation of  $S_\nu$  among three successive spatial points (Olson & Kunasz 1987). As described in Dullemond et al. (2002), we alternate the integration of the formal solution (i.e. ray-tracing) with the integration of the moment equations (eqs. [A13]–[A15]) and the determination of  $T$  by equation [A10] until we reach a convergence in  $T$  (the difference between the two successive iterations becomes less than 0.1%). In addition, we adopt the acceleration algorithm by Ng (1974) for a rapid convergence. For no scattering case, the convergence is very rapid independent of the total optical depth of the medium, typically 20 iterations. On the other hand, a factor of  $\sim 10$  times more iterations depending on the albedo are needed for isotropic scattering case.

### A4 Benchmark test

Figure A1 shows the result of the benchmark test No.3 proposed by C. P. Dullemond on his web page <sup>2</sup>. The settings are as follows: the stellar temperature  $T_* = 3,000$  K, the stellar radius  $R_* = 2.0 R_\odot$ , the distance from the star  $R = 1$  AU, the grazing angle  $\alpha = 0.05$ , the visible fraction of the stellar photosphere  $f_{\text{vis}} = 0.5$ , the total visual optical depth of the disc  $\tau_{0.55\mu\text{m}} = 10^4$  (i.e.  $\tau_{0.55\mu\text{m}} = 5 \times 10^3$  at the equatorial plane), and no scattering. We used the dust opacity model downloaded from the web page which is the same as that assumed in the calculation by C. P. Dullemond. The figure shows an excellent agreement between both results.

<sup>2</sup> <http://www.mpia-hd.mpg.de/homes/dullemond/radtrans/benchmarks/>

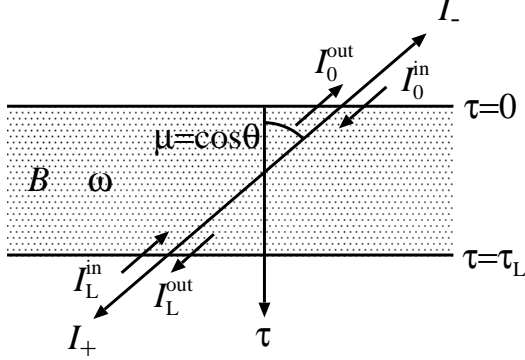


**Figure B1.** Plane-parallel isothermal medium with isotropic scattering.

## APPENDIX B: ANALYTIC EXPRESSION OF RADIATION FIELD IN ISOTHERMAL, ABSORPTION, AND ISOTROPIC SCATTERING MEDIUM

Here, we derive an analytic expression of the radiation field in an isothermal medium with absorption and isotropic scattering. In the derivation, we adopt the Eddington approximation with two-stream lines (e.g., Rybicki & Lightman 1979). We consider a diffuse incident radiation.

Suppose a plane-parallel medium (see Figure B1). We set the extinction (absorption+scattering) optical depth coordinate  $\tau$  along the normal of the medium. The total extinction optical depth of the medium is set to be  $\tau_L$ . Then, suppose that the single scattering albedo in this medium is  $\omega$  and this medium is isothermal and in the thermal equilibrium. The thermal radiation is denoted as  $B$ . Let us consider two-stream lines with the direction of  $\mu = \pm 1/\sqrt{3}$ , where  $\mu$  is the cosine of the angle between the ray and the  $\tau$  coordinate. When the direction of the rays is denoted by the subscript of + or -, the equation of the radiation transfer becomes

$$\pm \frac{1}{\sqrt{3}} \frac{dI_{\pm}}{d\tau} = S_{\pm} - I_{\pm}. \quad (\text{B1})$$

The source function can be expressed as

$$S_{\pm} = (1 - \omega)B + \omega J, \quad (\text{B2})$$

where  $J$  is the mean intensity. In the two-stream approximation, we can define the mean intensity  $J$ , the mean flux  $H$ , and the mean radiation pressure  $K$  as

$$J = \frac{1}{2}(I_+ + I_-), \quad (\text{B3})$$

$$H = \frac{1}{2\sqrt{3}}(I_+ - I_-), \quad (\text{B4})$$

and

$$K = \frac{1}{6}(I_+ + I_-) = \frac{1}{3}J. \quad (\text{B5})$$

The first and second moments of (B1) with the source function (B2) are

$$\frac{dH}{d\tau} = (1 - \omega)(B - J), \quad (\text{B6})$$

and

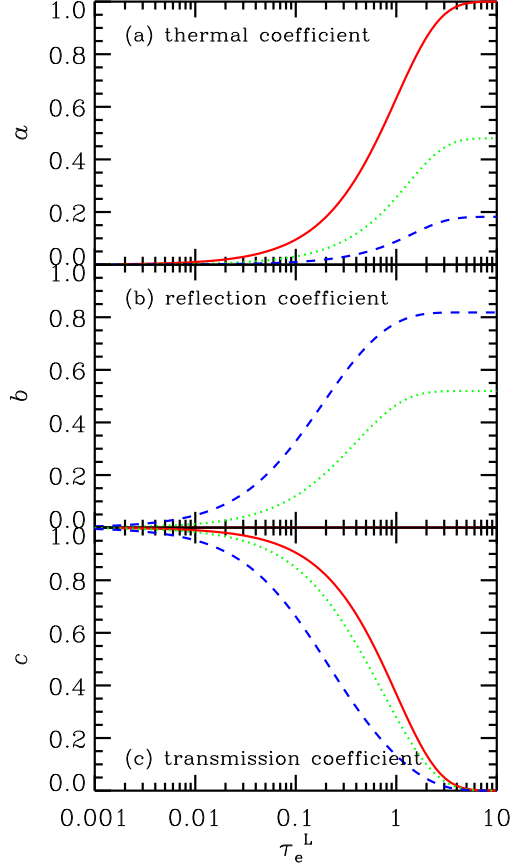


**Figure B2.** Thermal, reflection, and transmission coefficients as a function of effective optical depth of an isothermal, absorption, and isotropic scattering medium. In each panel, we show three cases of the single scattering albedo:  $\omega = 0$  (solid curve), 0.90 (dotted curve), and 0.99 (dashed curve). The reflection coefficient  $b$  is always zero when  $\omega = 0$ , so that we cannot see the solid curve in the panel (b). The effective optical depth  $\tau_e^L = \sqrt{3(1 - \omega)} \tau_L$  if the total (absorption+scattering) optical depth of the medium is  $\tau_L$ . Asymptotic values of the coefficients are given in equations (B17)–(B19).

$$\frac{1}{3} \frac{dJ}{d\tau} = -H. \quad (\text{B7})$$

With an effective optical depth  $\tau_e \equiv \tau \sqrt{3(1 - \omega)}$ , we have

$$\frac{d^2 J}{d\tau_e^2} = J - B, \quad (\text{B8})$$

from equations (B6) and (B7).

If we have incident radiations at the upper and lower boundaries as  $I_0^{\text{in}}$  and  $I_L^{\text{in}}$ , respectively, the boundary conditions are

$$J(0) = I_0^{\text{in}} + \sqrt{1 - \omega} \left( \frac{dJ}{d\tau_e} \right)_0, \quad (\text{B9})$$

and

$$J(\tau_e^L) = I_L^{\text{in}} - \sqrt{1 - \omega} \left( \frac{dJ}{d\tau_e} \right)_L, \quad (\text{B10})$$

where  $\tau_e^L = \tau_L \sqrt{3(1 - \omega)}$ . The solution of equation (B8)

with the boundary conditions (B9) and (B10) is

$$\begin{aligned}
 J(\tau_e) &= B \left[ 1 - \frac{e^{-\tau_e} + e^{-\tau_e^L + \tau_e}}{1 + \chi + (1 - \chi)e^{-\tau_e^L}} \right] \\
 &+ I_0^{\text{in}} \frac{(1 + \chi)e^{-\tau_e} - (1 - \chi)e^{-2\tau_e^L + \tau_e}}{(1 + \chi)^2 - (1 - \chi)^2 e^{-2\tau_e^L}} \\
 &+ I_L^{\text{in}} \frac{(1 + \chi)e^{-\tau_e^L + \tau_e} - (1 - \chi)e^{-\tau_e^L - \tau_e}}{(1 + \chi)^2 - (1 - \chi)^2 e^{-2\tau_e^L}}, \quad (\text{B11})
 \end{aligned}$$

where  $\chi = \sqrt{1 - \omega}$ . In the case without incident radiation (i.e.  $I_0^{\text{in}} = I_L^{\text{in}} = 0$ ), this solution is exactly same as equation (28) of Miyake & Nakagawa (1993).

Then, let us consider the outbound intensity at the surface of the medium. At  $\tau = 0$ , the outbound intensity can be

$$I_0^{\text{out}} = aB + bI_0^{\text{in}} + cI_L^{\text{in}}, \quad (\text{B12})$$

where  $a$ ,  $b$ , and  $c$  can be called as ‘‘thermal’’, ‘‘reflection’’, and ‘‘transmission’’ coefficients, respectively. Since  $J(0) = (1/2)(I_0^{\text{in}} + I_0^{\text{out}})$ , we obtain from equation (B11)

$$a = \frac{2\chi(1 - e^{-\tau_e^L})}{1 + \chi + (1 - \chi)e^{-\tau_e^L}}, \quad (\text{B13})$$

$$b = \frac{(1 - \chi)(1 + \chi)(1 - e^{-2\tau_e^L})}{(1 + \chi)^2 - (1 - \chi)^2 e^{-2\tau_e^L}}, \quad (\text{B14})$$

and

$$c = \frac{4\chi e^{-\tau_e^L}}{(1 + \chi)^2 - (1 - \chi)^2 e^{-2\tau_e^L}}. \quad (\text{B15})$$

At  $\tau = \tau_L$ , we obtain symmetrically

$$I_L^{\text{out}} = aB + bI_L^{\text{in}} + cI_0^{\text{in}}. \quad (\text{B16})$$

Figure B2 shows the three coefficients for an isotropic case as a function of the effective optical depth of the medium  $\tau_e^L$ . As limiting values, we obtain

$$a \rightarrow \begin{cases} \frac{2\chi}{1 + \chi} & (\tau_L \rightarrow \infty) \\ 0 & (\tau_L \rightarrow 0) \end{cases}, \quad (\text{B17})$$

$$b \rightarrow \begin{cases} \frac{1 - \chi}{1 + \chi} & (\tau_L \rightarrow \infty) \\ 0 & (\tau_L \rightarrow 0) \end{cases}, \quad (\text{B18})$$

and

$$c \rightarrow \begin{cases} 0 & (\tau_L \rightarrow \infty) \\ 1 & (\tau_L \rightarrow 0) \end{cases}. \quad (\text{B19})$$